

Folding Pathways of Prion and Doppel

Gianni Settanni*, Trinh Xuan Hoang^{*,†}, Cristian Micheletti* and Amos Maritan^{*,†,**}

**International School for Advanced Studies (S.I.S.S.A.) and INFN, Via Beirut 2-4, 34014*

Trieste, Italy; †The Abdus Salam International Center for Theoretical Physics (ICTP), Strada

Costiera 11, 34100 Trieste, Italy

(November 13, 2018)

*** Corresponding author:*

Amos Maritan

International School for Advanced Studies (SISSA/ISAS)

via Beirut 2-4

34014 Trieste

ITALY

tel: +39.040.2240462

fax: +39.040.3787528

email: maritan@sissa.it

Abstract

The relevance of various residue positions for the stability and the folding characteristics of the prion protein are investigated by using molecular dynamics simulations of models exploiting the topology of the native state. Highly significant correlations are found between the most relevant sites in our analysis and the single point mutations known to be associated with the arousal of the genetic forms of prion disease (caused by the conformational change from the cellular to the scrapie isoform). Considerable insight into the conformational change is provided by comparing the folding process of prion and doppel (a newly discovered protein) sharing very similar native state topology: the folding pathways of the former can be grouped in two main classes according to which tertiary structure contacts are formed first enroute to the native state. For the latter a single class of pathways leads to the native state. Our results are consistent and supportive of the recent experimental findings that doppel lacks the scrapie isoform and that such remarkably different behavior results from differences in the region containing the two β -strands and the intervening helix.

I. INTRODUCTION

Neurodegenerative diseases causing transmissible spongiform encephalopathies (TSE) are the subject of intense research. They affect humans and animals and include scrapie in sheep, mad-cow disease in bovines and Creutzfeldt-Jacob disease in humans. Most of them arise sporadically, the rest of the instances are inherited or transmitted by inoculation through the dietary or infected tissues.

The belief is that the normal, and benign, form of the prion protein PrP^c , which is found in various organs of vertebrates, including the brain, can undergo a post translational process leading to a conformational change of its native state [1]. This new form is designated PrP^{sc} and contrarily to PrP^c it is insoluble. The NMR investigation of the three-dimensional structure of recombinant PrP^c of various species [2–10] has revealed that the N-terminus is unstructured whereas the C-terminus consists of three α -helices and two short β -strands.

On the other hand the structure of the malign form, PrP^{sc} , is mostly unknown. However, spectroscopic investigations, mainly based on circular dichroism, showed that PrP^c contains about 40% α -helices and little β -sheet, whereas PrP^{sc} is composed of about 30% α -helices and 45% β -sheet [11,12].

Unfolding and re-folding experiments suggest that the conversion between the α -rich and β -rich form occurs through a complete unfolding of the protein [13]. Experiments and clinical tests suggest two main processes for the onset and spreading of the prion infection. In the first case, the spreading of the scrapie form in healthy tissues contaminated with PrP^{sc} reveals that the presence of PrP^{sc} helps further conversion from normal to scrapie form, i.e. PrP^{sc} acts as a template for the restructuration of PrP^c . In the second case, the genetic influence on the propensity of cellular PrP^c to rearrange into PrP^{sc} is revealed by the discovery of, at least, 20 single point mutations in the PrP gene in Humans which favor the spontaneous onset of the disease [4,5,14–16].

Within the picture presented in [13] the role of the mutations in the arousal of the disease could be caused by several factors ranging from the lowering of a free energy barrier in the conversion process to the increase in the oligomerization rate. One of the goals of the present study is to understand which are the sites where mutations are expected to have the major impact in the stabilization/destabilization of the PrP^c structure and/or its folding process.

Recently, some experiments on transgenic mice lacking the PrP gene ($PrnP^{0/0}$) have revealed the onset of neurodegeneration (Purkinje-cell death) [17] completely different from usual prion disease. This disease was ultimately traced back to a prion homologous gene, $Prnd$, (not expressed in normal subjects), which encoded a protein named doppel, Dpl which has almost the same topology of PrP^c , despite the low sequence identity (25%).

A striking difference between Dpl and PrP^{sc} , is that the former affects the central nervous system while retaining its native structure, i.e. without a need to convert to a scrapie-like conformation. Various hypothesis have been formulated [18] to explain these different behaviours.

The theoretical framework we elaborated and adopted in our study helps to shed light on the putative causes for such remarkably different behavior of doppel and prion. Indeed, the different folding behavior and stability of prion and doppel are related, at least in part, to the small, but important, differences in the topology of the native state which affect in an amplified fashion, the folding routes and ultimately facilitating structural rearrangements of prion.

The model we adopt builds on the importance of the native state topology in steering the folding process, that is in bringing into contact pairs of amino acids that are found in interaction in the native state. In the past few years an increasing amount of experimental [19–21] and theoretical [22–30] evidence (such as all-atom molecular dynamics (MD) simulations in implicit solvent) have confirmed this view [31,32].

A further confirmation of this view is provided by the remarkable accord of the key folding stages predicted by topology-based models and the available experimental results [33,34]. Indeed, the success of the topological picture itself helps to explain why the folding process is not too sensitive to the detailed chemical composition of most residues in a protein. The dependence of the folding process on the detailed chemistry is much more subtle than that given by the native state topology.

Usually the folding mechanism is affected only when mutations occurs in a small set of key residues. Within our theoretical framework those key residues take part to contacts that are crucial for the folding process [33].

The establishment of the key contacts leads to a rapid formation of further interactions. Interestingly, the folding bottlenecks can be identified by just knowing the topology of the native conformation [33,34]. Thus, the topology itself also dictates the impact of chemistry on the folding process.

The purpose of the present work is three-fold:

i) determination of the folding bottlenecks for the cellular prion and the identification of the key amino acids taking part to the corresponding crucial contacts;

ii) making connection between the set of such key residues with those that are known to be associated with harmful PrP^{sc} mutations. As argued before, a random mutation on key positions will usually result in a disruption of the folding process. Only fine-tuned mutations can lead to a wild-type-like native state (as for viral enzymes mutating under drug attack

[33]) or in another viable structure (as postulated by Prusiner for the prion [1]);

iii) furthermore, we will focus our attention on how the topological differences between the native states of Dpl and PrP^c may have impact on the folding process thus aiding or avoiding the formation of misfolded conformers. It is important to stress that our study is based on the native-state structures of PrP^c and Dpl . Hence, although we can confidently identify the crucial folding residues, we cannot confirm explicitly that their mutation results in a different native state form.

II. MATERIALS AND METHODS

A. The model for prion

Our model builds on a schematic representation of the three-dimensional structure of the protein, where the amino acids are replaced by effective centroids identified with the C_α atoms. The bias towards the native state is introduced through a Go-like [35] energy scoring function that rewards the formation of native contacts between the centroids. The list of native interactions was compiled from the knowledge of the coordinates of atoms of the human prion protein (PDB code 1qlx). A pair of amino acids is considered in interaction if any pair of their heavy atoms, i and j , have a native separation smaller than the distance, $1.244(R_i + R_j)$, where the point of inflection of the Van der Waals interaction occurs (R_i denotes the Van der Waals radius of atom i). The values of R_i are taken from Ref. [36]. In this way one defines a symmetric matrix, known as contact map, Δ , whose entries, Δ_{ij} are equal to 1 if the i -th and j -th centroids interact, and zero otherwise.

The energy function for our system includes terms that are routinely used in standard molecular dynamics (MD) simulations on biopolymers [37,38]. It is composed by a "bonded" and a "non-bonded" term: $E = V_B + V_{NB}$. The former accounts for the constraints such as the peptide bond length and Ramachandran angles bias acting on the aminoacids at a local level. Its explicit form is:

$$V_B = g \cdot V_p + h \cdot V_a + k \cdot V_d, \quad (1)$$

$$V_p = \sigma \sum_{i=1}^{N-1} \left(r_{i,i+1} - r_{i,i+1}^{(n)} \right)^2, \quad (2)$$

$$V_a = \sigma \sum_{i=1}^{N-2} \left(\theta_{i,i+1,i+2} - \theta_{i,i+1,i+2}^{(n)} \right)^2, \quad (3)$$

$$V_d = \sigma \sum_{i=1}^{N-3} \left(1 - \cos \left(\tau_{i,i+1,i+2,i+3} - \tau_{i,i+1,i+2,i+3}^{(n)} \right) \right), \quad (4)$$

where $r_{i,j}$ is the distance between residue i and j , $\theta_{i,j,k}$ is the angle with the j -th amino acid as vertex and the i -th and the k -th as edges and $\tau_{i,j,k,l}$ is the dihedral generated by the i -th, the j -th, the k -th and the l -th amino acid. The n as superscript denotes the native state value. σ represents a suitable scale factor to fix the temperature scale (set to 10 in our simulations) which is given in dimensionless units.

The minimum of expression (1) is precisely attained in correspondence of the native state. However the cooperative character of the folding process [39] can be captured only

by introducing an explicit bias towards the formation of native interactions [40]. This is accomplished through the second term, V_{NB} , which weights the interaction of any pair of non-consecutive centroids with a Van der Waals-like potential:

$$V_{NB} = \sigma \sum_{i < j-3}^N V_{ij} = \sigma \sum_{i < j-3}^N \left(5 \left(\frac{r_{ij}}{r_{ij}^{(n)}} \right)^{-12} - 6 \left(\frac{r_{ij}}{r_{ij}^{(n)}} \right)^{-10} \Delta_{ij} \right). \quad (5)$$

This choice rewards native interactions and disfavors non-native ones. The form of the energy scoring function ensures that the global minimum is attained in correspondence of the native state, regardless of the precise values for the (positive) couplings parameters g , h , k . The values used in the present study are: $g = 50$, $h = 5$ and $k = 0.3$; we have checked that the results are robust to their variation within a certain range [34].

The dimensionless unit of time in our MD simulations is $5 \cdot 10^{-3}$ and conformations were sampled every 500 time steps to allow a sufficient uncorrelation at temperatures below the folding transition. The multiple-histogram technique [41] has been applied to reweight quantities such as the average internal energy collected in more than 50 equilibrated runs at different temperatures in the range 2-8. The optimal reweighting allows to calculate thermodynamic quantities, such as the average internal energy and the specific heat for an arbitrary temperature, T .

As visible in Fig. 1A, the specific heat exhibits a single peak which signals the folding transition [42]. In addition to this overall characterization of the equilibrium thermodynamics, it is possible to monitor how the individual interactions that are present in the native state are formed as the folding progresses. Indeed, although all native contacts are energetically favored in the same way, their entropic cost of formation may significantly vary according to their locality, burial/exposure etc. .

The crucial contacts for the folding process are identified according to the method given in Refs. [33,34,40], which singles out the contacts giving the largest contribution to the overall specific heat at the folding transition temperature, T_F .

$$c_{ij} = \frac{d\langle V_{ij} \rangle}{dT} = (\langle V_{NB} V_{ij} \rangle - \langle V_{NB} \rangle \langle V_{ij} \rangle) / kT^2 \quad (6)$$

The physical interpretation of this procedure is that these special contacts are precisely those that, having a significant and sudden formation at T_F , act as bottlenecks for the folding process. $c_{i,j}$ measures the sensitivity of the average energy of the system to perturbation occurring at the contact (i, j) .

In our studies, a long run carried out at T_F of $2 \cdot 10^7$ time steps, allowed a detailed analysis for all contacts. In addition to the identification of crucial contacts, it is useful to introduce a similar measure for the individual amino acids through the single residue specific heat (SRSH) resulting from the contribution of all contacts to which a given site, i , takes part to:

$$c_i = \sum_j \Delta_{ij} c_{ij} \quad (7)$$

SRSH's have been used to identify folding and unfolding phases and to pinpoint residues that play a relevant role in the process [33,34]. The crucial folding steps can thus be identified with two (related) criteria: namely either through the contacts or the sites with the largest specific heat of formation.

B. Folding pathways

Another issue that we have addressed in our study is to establish the presence of alternative pathways taking from unfolded conformations to the native state. Again, this is accomplished by examining in detail both the thermodynamic and the kinetic relevant features extracted from the model. The comparison of dynamic trajectories connecting unfolded and native-like conformations has revealed the presence of several folding events that have to occur for the protein to fold. The main ones that emerged from our analysis, and that are particularly apt for characterizing the folding process, correspond to the formation of contacts involving three sets of contiguous residues. The first set, Bh , from residue 125 to residue 172 comprises all N-terminal residues (β -sheet included) before the helix 2 (defined according to the indications in the PDB file). The second set, $h1$, from residue 173 to 194 comprises residues of helix 2, and finally the third set, $h2$, from residue 200 to 228 is composed of residues from helix 3.

The four observed events are:

- Event Bh : formation of contacts between residues within Bh ,
- Event $Bh-h1$: formation of contacts between Bh and $h1$,
- Event $Bh-h2$: formation of contacts between Bh and $h2$,
- Event $h1-h2$: formation of contacts between $h1$ and $h2$.

For convenience of presentation, in order to describe the four events on a similar footing, we focus on the top 10 contacts (in terms of specific heat contributions c_{ij}) in each interacting group. It is interesting to note that, among this top contacts, those occurring within an α helix almost never occur. This can be explained since local contacts, among others, are easily formed, even at high temperature, and hence do not constitute a bottleneck for overcoming the configurational barrier to the native state.

We computed the fraction of formed contacts, Q_i ($i = Bh, Bh-h1, Bh-h2, h1-h2$), within each of the 4 groups along the dynamical trajectories of $2 \cdot 10^7$ steps at T_F . The natural binning size for each of the Q_i was 1/10. From this, we obtained a vivid picture of the dynamical effects of the free energy landscape at the folding transition (see Fig. 5 and the Results section).

We also carried out 100 (“quenched”) folding runs at $T = (1 - \epsilon)T_F$, where $\epsilon = 1/30$, slightly below T_F , starting from completely unfolded conformations (thermalised at high temperature runs). In all cases, the native state was reached in less than $2 \cdot 10^5$ steps. The average Q_i ’s as a function of the elapsed time using all 100 trajectories was also calculated (Fig. 5).

C. Doppel protein

We carried out a parallel analysis for the doppel protein, Dpl , whose NMR-resolved structure was retrieved from the PDB (PDB code 1i17, model 1). For this protein too, we built the contact map considering all-atom distances, and obtained both the overall specific

heat (Fig. 1B) and the one associated to individual contacts using the same methods described above. A crucial difference in the folding events of the two proteins was revealed by monitoring the four events, analogous to those of the previous section.

For *Dpl* the sets of amino acids structurally homologous of the prion ones are as follows: the set *Bh* corresponds to residues from 1 to 50 before helix 3; *h1* to residues from 51 to 76 (comprising helix 3 and 4) and the set *h2* to residues from 78 to 96 (comprising helix 5). The numeration of the helices is consistent with the secondary structure indications present in the PDB file. Free energy profiles and time dependent averages of the reaction coordinate are shown in Fig. 4 and 5 respectively.

III. RESULTS

A. Determination of key residues

The specific heat curves as a function of the temperature for *PrP^c* and *Dpl* are shown in Figures 1A and 1B, respectively. The single peak in each of them allows to identify unambiguously the folding transition in these systems.

From the long run of $2 \cdot 10^7$ time steps performed at T_F , the SRSH's for prion have been computed according to eq.(7). We have ranked the residues according to their SRSH (see Table 1). It is natural to compare the top key sites from our analysis with those whose mutation is known to favor the emergence of *PrP^{sc}* (highlighted in Table 2). In the top 10 amino acids of our list we found 4 of the known key mutating sites; whereas in the top 30 amino acids their number increases to 12. The statistical relevance of this match can be obtained from a combinatorics calculation of the probability to have at least the observed number of matches by pure chance. For the top 10 amino acids the probability to get a better results by chance is 6.8% whereas for the top 30 amino acids that probability becomes 0.02%. Thus, the criterion based on the SRSH allows to identify confidently amino acids important for the folding process of the prion protein.

Their structural location and role is made apparent in Fig. 2 where the prion contact map has been colored according to the value of the SRSH. As visible, crucial contacts connect secondary-structure elements thus forming the protein tertiary structure. In particular they connect the β -sheet-helix-1 region to the helix-2 and helix-3 (*Bh-h1* and *Bh-h2* sets, respectively) and helix-2 - helix-3 (*h1-h2* set). The parts of the protein contributing more to the specific heat, within our model, are located at the C-terminal strand of the β -sheet, and at the two C-terminal helices, especially helix-3 (see Fig. 3).

B. Folding pathways

The analysis of the long run of $2 \cdot 10^7$ time steps carried out at T_F has led to the construction of an *effective* free energy landscape. It is based on the reaction coordinates Q_i as defined in the Methods section. The free energy as a function of pairs (Q_i, Q_j) for all six combinations of i and j have been calculated as

$$F(Q_i, Q_j) = - \ln (P(Q_i, Q_j)) \tag{8}$$

where $P(Q_i, Q_j)$ is the fraction of times the dynamical trajectory spends in the bin around (Q_i, Q_j) . The contour plots of F are shown in Figures 4A and 4B for PrP^c and Dpl respectively. The two energy minima around $Q = 0$ and in the higher Q region correspond to the unfolded and (partially) folded conformations respectively. For prion the plots involving set $h1-h2$ show the presence of multiple pathways connecting these two minima. For example, the contour plot in the bidimensional space spanned by Q_{h1-h2} and Q_{Bh-h1} presents two possible successions of events: either the $Bh-h1$ set is formed followed by formation of $h1-h2$ set or *vice versa* (see Fig. 4A). The same observation can be done for the other plots involving set $h1-h2$. Such pathway ambiguity is absent for the case of doppel (Fig. 4B), where trajectories can be grouped essentially in a single set. Indeed, for doppel, on average, the formation of the $h1-h2$ contacts follows the other sets. This result is further confirmed by the analysis of the time-dependent average of the reaction coordinates Q_i 's as obtained from the 100 non-equilibrium folding runs. Figures 5A and 5B show the results for PrP^c and Dpl respectively. For Dpl the order in the formation of the contacts is the same detected by the equilibrium run: set Bh is formed before set $Bh-h1$ that is followed by $Bh-h2$ eventually followed by $h1-h2$ interhelical contacts. On the other hand, such definite succession of events is not observed for prion.

IV. DISCUSSION

The goal of our numerical study was to characterize the folding process of the prion protein elucidating the structural mechanisms responsible for the propensity of PrP^c to mutate into the harmful scrapie form, PrP^{sc} .

At the heart of our analysis is a topology-based energy function that, by rewarding the formation of native-like interactions among the residues, allows to mimic the progressive build-up of native structure in a folding process. Remarkably, the progress towards the native state does not advance smoothly, but occurs through the overcoming of configurational barriers, which are responsible for the appearance of a marked peak in the specific heat curve. Crucial contacts (and sites) for the folding process have thus been identified as those giving the largest contributions to the specific heat peak (Fig. 2).

The top sites isolated by our procedure contain a highly significant fraction of residues that are known to enhance the misfolding propensity of PrP^c . This indicates that there is little freedom in choosing the chemical identity of the amino acids at the sites which have a special structural role during the folding process.

The analysis presented here, based on topological arguments, provides a physically appealing interpretation for the connection between certain site mutations and the arousal of the prion disease. Conversely, the key mutating sites not captured by our analysis are presumably crucial because they affect some aspects of the process leading to the scrapie form that cannot be accounted for by the present method. For example, the alternative mechanism leading to misconformation is the template binding of PrP^c to PrP^{sc} involving the interconversion of the former into the latter one. Consistently with this interpretation, amino acids that do not present high SRSH and that are known to be involved in the development of the disease, specifically MET 129, GLU200 and GLU 219, (i.e. mostly charged residues with a large exposed surface area).

Despite the substantial topological similarities of *Dpl* and *PrP^c*, the detailed analysis of the folding trajectories of both proteins have revealed significant differences of the folding pathways. Strikingly, for *PrP^c* the folding pathways can be classified in two main distinct routes, whereas for *Dpl* only one of these is essentially present. For the latter, the series of folding steps is more distinctly marked than for the former. Such noticeably different behavior can be ascribed to the different set of contacts stabilizing the assembly of the α -helices and β -sheets in the two proteins. It is interesting to note that the contact order [21] of *PrP^c* is 0.2056 and is lower than that of *Dpl* which is 0.2298, even though the former has somewhat higher number of contacts which is, in turn, reflected by the shift of the folding transition peak towards higher temperatures (see Fig. 1). This difference could explain the different average folding time measured in our models for the two proteins. Indeed, according to Fig. 5, the sets of contacts in prion are all formed within the first 25000 time steps while contacts in doppel contacts can take 4-5 times longer to form. This difference is of the same order of magnitude of that predicted by Plaxco [21] on the basis of the contact order of the two proteins. Although the present picture would certainly be influenced by the introduction of amino acid specific interactions, it is appealing to connect the different folding routes to the appearance of misfolded conformers. According to this view, the latter would result from following the folding route of *PrP^c* where the inter C-terminal helices contacts (set *h1-h2*) are formed while the contacts with the β -sheet (set *Bh-h1* and *Bh-h2*) are not yet formed (Figures 4A and 5A). Indeed, along this route, which is alternative to the one where the two events are interchanged as it occurs in the single route of doppel (Fig. 4B and 5B), the N-terminal part of the protein is free to rearrange its structure before reaching the native-state. This scenario is consistent with several recent models (see e.g. Ref. [43,44]) that identify the N-terminal part of the protein as the one that undergoes the conformational change that leads the scrapie form of prion.

REFERENCES

- [1] Prusiner S.B. (1982) *Science*, **216**, 136-144.
- [2] Goldgaber, D., Goldfarb, L. G., Brown, P., Asher, D. M., Brown, W. T., Lin, S., Teener, J. W., Feinstein, S. M., Rubenstein, R., Kascsak, R.J. et al. (1989) *Exp. Neurol.* **106**, 204-206.
- [3] Kretzschmar, H. A., Honold, G., Seitelberger, F., Feucht, M., Wessely, P., Mehraein, P. & Budka, H. (1991) *Lancet* **337**, 1160.
- [4] Hsiao, K., Baker, H. F., Crow, T. J., Poulter, M., Owen, F., Terwilliger, J. D., Westaway, D., Ott, J. & Prusiner, S. B. (1989) *Nature* **338**, 342-345.
- [5] Gabizon, R., Rosenmann, H.,Meiner, Z., Kahana, I., Kahana, E., Shugart, Y., Ott, J. & Prusiner, S. B. (1993) *Am. J. Hum. Genet.* **53**, 828-835.
- [6] Calzolari, L., Lysek, D. A., Guntert, P., von Schroetter, C., Riek, R., Zahn, R. & Wuthrich, K. (2000) *Proc. Natl. Acad. Sci. USA* **97**, 8340-834.
- [7] Lopez, G. F., Zahn, R., Riek, R. & Wuthrich, K. (2000) *Proc. Natl. Acad. Sci. USA* **97**, 8334-8339.
- [8] Liu, A., Riek, R., Wider, G., von Schroetter, C., Zahn, R. & Wuthrich, K. (2000) *J. Biomol. NMR* **16**, 127-138.
- [9] Zahn, R., Liu, A., Luhrs, T., Riek, R., von Schroetter, C., Lopez, G. F., Billeter, M., Calzolari, L., Wider, G. & Wuthrich, K. (2000) *Proc. Natl. Acad. Sci. USA* **97**, 145-150.
- [10] James, T. L., Liu, H., Ulyanov, N. B., Farr-Jones, S., Zhang, H., Donne, D. G., Kaneko, K., Groth, D., Mehlhorn, I., Prusiner, S. B. et al. (1997) *Proc. Natl. Acad. Sci. USA* **94**, 10086-10091.
- [11] Pan, K. M., Baldwin, M., Nguyen, J., Gasset, M., Serban, A., Groth, D., Mehlhorn, I., Huang, Z. W., Fletterick, R. J., Cohen, F. E. et al. (1993) *Proc. Natl. Acad. Sci. USA* **90**, 10962-10966.
- [12] Pergami, P., Jaffe, H. & Safar, J. (1996) *Anal. Biochem.* **236**, 63-73.
- [13] Baskakov, I. V., Legname, G., Prusiner, S. B. & Cohen, F. E. (2001) *J. Biol. Chem.* **276**, 19687-19690.
- [14] Dlouhy, S. R., Hsiao, K., Farlow, M. R., Foroud, T., Conneally, P. M., Johnson, P., Prusiner, S. B., Hodes, M. E. & Ghetti, B. (1992) *Nat. Genet.* **1**, 64-67.
- [15] Petersen, R. B., Tabaton, M., Berg, L., Schrank, B., Torack, R. M., Leal, S., Julien, J., Vital, C., Deleplanque, B., Pendlebury, W. W. et al. (1992) *Neurology* **42**, 1859- 1863.
- [16] Poulter, M., Baker, H. F., Frith, C. D., Leach, M., Lofthouse, R., Ridley, R. M., Shah, T., Owen, F., Collinge, J., Brown, J. et al. (1992) *Brain* **115**, 675- 685.
- [17] Sakaguchi, S., Katamine, S., Nishida, N., Moriuchi, R., Shigematsu, K., Sugimoto, T., Nakatani, A., Kataoka, Y., Houtani, T., Shirabe, S. et al. (1996) *Nature* **380**, 528-531.
- [18] Mo, H., Moore, R. C., Cohen, F. E., Westaway, D., Prusiner, S. B., Wright, P. E. & Dyson, H. J. (2001) *Proc. Natl. Acad. Sci. USA* **98**, 2352-2357.
- [19] Riddle, D. S., Grantcharova, V. P., Santiago, J. V., Alm, E., Ruczinski, I., I & Baker, D. (1999) *Nat. Struct. Biol.* **6**, 1016-1024.
- [20] Martinez, J. C. & Serrano, L. (1999) *Nat. Struct. Biol.* **6**, 1010-1016.
- [21] Plaxco, K. W., Simons, K. T. & Baker, D. (1998) *J. Mol. Biol.* **277**, 985-994.
- [22] Micheletti, C., Banavar, J. R., Maritan, A. & Seno, F. (1999) *Phys. Rev. Lett.* **82**, 3372-3375.
- [23] Maritan, A., Micheletti, C. & Banavar, J. R. (2000) *Phys. Rev. Lett.* **84**, 3009-3012.

- [24] Maritan, A., Micheletti, C., Trovato, A. & Banavar, J. R. (2000) *Nature* **406**, 287-290.
- [25] Baker, D. (2000) *Nature* **405**, 39-42.
- [26] Munoz, V. & Eaton, W. A. (1999) *Proc. Natl. Acad. Sci. USA* **96**, 11311-11316.
- [27] Alm, E. & Baker, D. (1999) *Proc. Natl. Acad. Sci. USA* **96**, 11305-11310.
- [28] Galzitskaya, O. V. & Finkelstein, A. V. (1999) *Proc. Natl. Acad. Sci. USA* **96**, 11299-11304.
- [29] Clementi, C., Nymeyer, H. & Onuchic, J. N. (2000) *J. Mol. Biol.* **298**, 937-953.
- [30] C. Micheletti, SISSA preprint (2001).
- [31] Ferrara, P. & Caffisch, A. (2001) *J. Mol. Biol.* **306**, 837-850.
- [32] Gsponer, J. & Caffisch, A. (2001) *J. Mol. Biol.* **309**, 285-298.
- [33] Cecconi, F., Micheletti, C., Carloni, P. & Maritan, A. (2001) *Proteins* **43**, 365-372.
- [34] Settanni G, Cattaneo A & Maritan A, (2001) *Biophys. Journ.* **80** 2935-2945
- [35] Go, N. (1983) *Annu. Rev. Biophys. Bioeng.* **12**, 183-210.
- [36] Tsai, J., Taylor, R., Chothia, C. & Gerstein, M. (1999) *J. Mol. Biol.* **290**, 253-266.
- [37] Pearlman, D. A., Case, D. A., Caldwell, J. W., Ross, W. S., Cheatham, T. E., Debolt, S., Ferguson, D., Seibel, G. & Kollman, P. (1995) *Computer Physics Communications* **91**, 1-41.
- [38] Brooks, B. R., Bruccoleri, R. E., Olafson, B. D., States, D. J., Swaminathan, S. & Karplus, M. (1983) *J. Comp. Chem.* **4**, 187-217.
- [39] Kaya, H. & Chan, H. S. (2000) *Phys. Rev. Lett* **85**, 4823-4826; Kaya, H. & Chan, H. S. (2000) *Proteins* **40**, 637-661.
- [40] Micheletti, C., Banavar, J. R. & Maritan, A. (2001) *Phys. Rev. Lett.* **87**, art. no. 088102
- [41] Ferrenberg, A. M. & Swendsen, R. H. (1989) *Phys. Rev. Lett.* **63**, 1195-1198.
- [42] Hao, M. H. & Scheraga, H. A. (1997) *Physica A* **244**, 124-146.
- [43] Peretz, D., Williamson, R. A., Matsunaga, Y., Serban, H., Pinilla, C., Bastidas, R., Rozenshteyn, R., James, T. L., Houghten, R. A., Cohen, F. E., *et al* (1997) *J. Mol. Biol.* **273**, 614-622.
- [44] Huang, Z., Prusiner, S. B. & Cohen, F. E. (1996) *Fold. Des.* **1**, 13-19.

TABLES

rank	site	rank	site	rank	site
1	137	11	213	21	214
2	210	12	165	22	163
3	175	13	160	23	212
4	158	14	162	24	184
5	141	15	206	25	187
6	183	16	205	26	179
7	209	17	157	27	208
8	198	18	139	28	217
9	161	19	150	29	159
10	211	20	134	30	180

TABLE I. Top 30 sites in prion ranked according to the single residue specific heat (SRSH).

145, <u>160</u> , 178, <u>179</u> , <u>180</u> , 183 , <u>187</u> , 188, 196, 198 , 200, 202, <u>208</u> , 210 , 211 , <u>212</u> , <u>214</u> , <u>217</u>
--

TABLE II. Sites where mutations (in the NMR-solved part of Human *PrP*) have been observed to cause/stop the prion disease or be fundamental for correct folding of *PrP^c*. Sites 214 and 179 represent cysteine residues that form a disulfide bond needed to observe the *PrP^c* α -form of prion [32]. Single residue specific heat (SRSH), as determined by our model, ranking within the top 10 are in boldface; those ranking within the top 30 are underlined (see Table 1).

Figure captions

1. Figure 1. Temperature dependent specific heat for the prion (A) and doppel (B) models. The folding transition temperature is identified at the point where the specific heat peak occurs.
2. Figure 2. Contact map of PrP^c (PDB code 1qlx) where contacts are highlighted according to their specific heat c_{ij} of equation (6). Red spots correspond to contacts with high c_{ij} , while blue ones correspond low SRSH. The relevant sets of contacts (as defined in the text) are framed within the rectangles; (a) set Bh , (b) set $Bh-h1$, (c) set $Bh-h2$, (d) set $h1-h2$. Notice that red spots are prevalent in all sets but Bh .
3. Figure 3. The three-dimensional structure of prion protein where amino acids have been colored according to the value of their SRSH. Red spots are located mainly on the C-terminal strand of the β -sheet, on helix-2 and helix-3.
4. Figure 4. Effective free energy landscape for prion (A) and doppel (B) model. Upper and right squares represent the contact maps where the representative set of contacts defining the reaction coordinates are highlighted (see Method section). Contour plots are shown for each of the six pairs of reaction coordinates (Q_i, Q_j) . White (black) spots represent low (high) values of the free energy. The minimum close to (0,0) corresponds to the unfolded state whereas the minimum closer to (1,1) corresponds to the folded state. In most of the contour plots for prion (A) more than one class of favorable paths from the unfolded to the folded conformation is possible whereas for doppel (B) only one class of paths is the most favorable. Following these pathways allows to assign a preferential order to the events. Thus, on average, the sequence of contact formation for doppel is Bh , $Bh-h1$, $Bh-h2$ and $h1-h2$ (see also Fig. 5). For prion, two class of equivalent pathways are present: in one case the $h1-h2$ contacts are formed before the other sets of contacts; in the other case $h1-h2$ contacts follow the formation of all the other contacts as for Dpl .
5. Figure 5. Average time dependence of reactions coordinates Q_i 's for prion (A) and doppel (B) computed on 100 folding runs starting from completely unfolded conformations. (A) In case of prion the curves corresponding to the different sets (red for Bh , green for $Bh-h1$, blue for $Bh-h2$ and magenta for $h1-h2$) present intersections. Indeed the average over the different folding pathways results in a non well-defined sequence of folding events (B) The folding events in the case of doppel protein have a well defined sequence: Bh set (red) is the first to form; then $Bh-h1$ (green); then $Bh-h2$ (blue); finally $h1-h2$ (magenta).

FIGURES

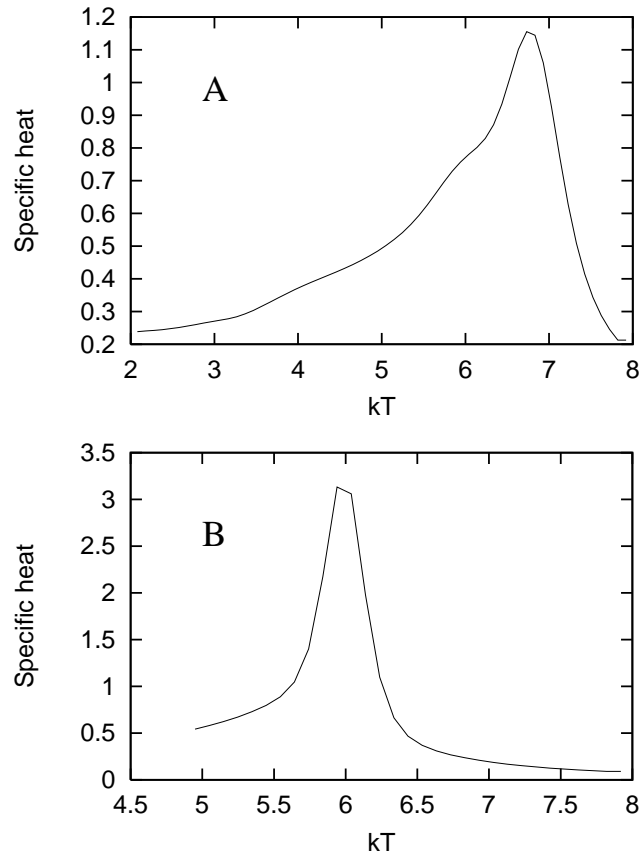


FIG. 1.

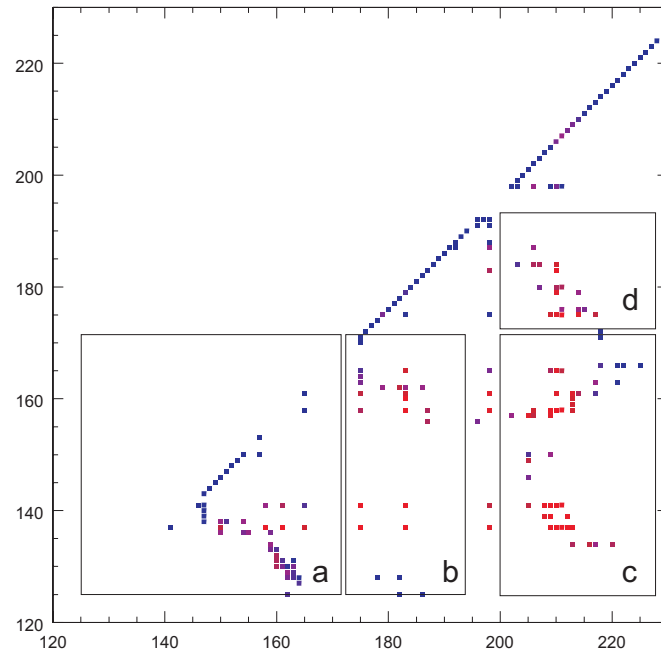


FIG. 2.

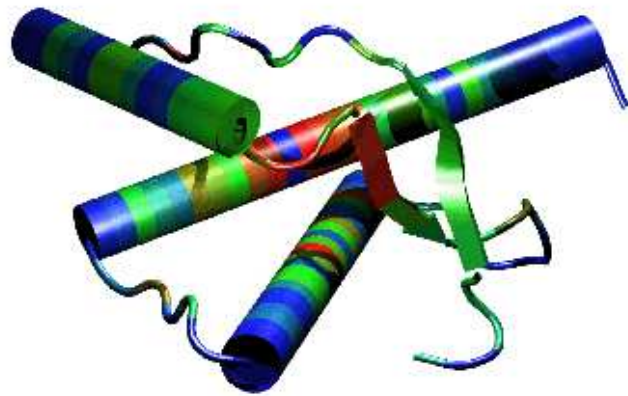


FIG. 3.

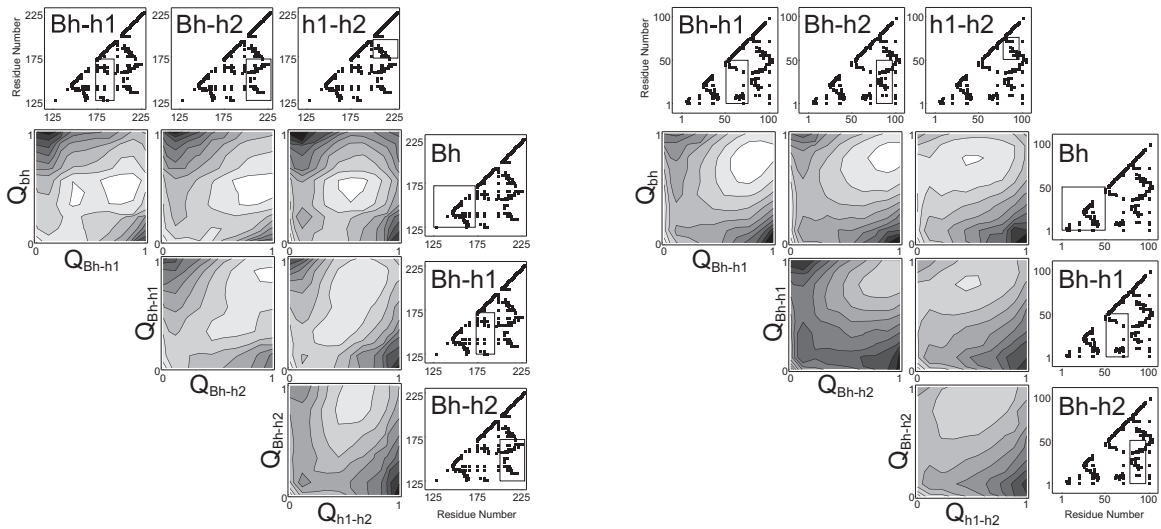


FIG. 4.

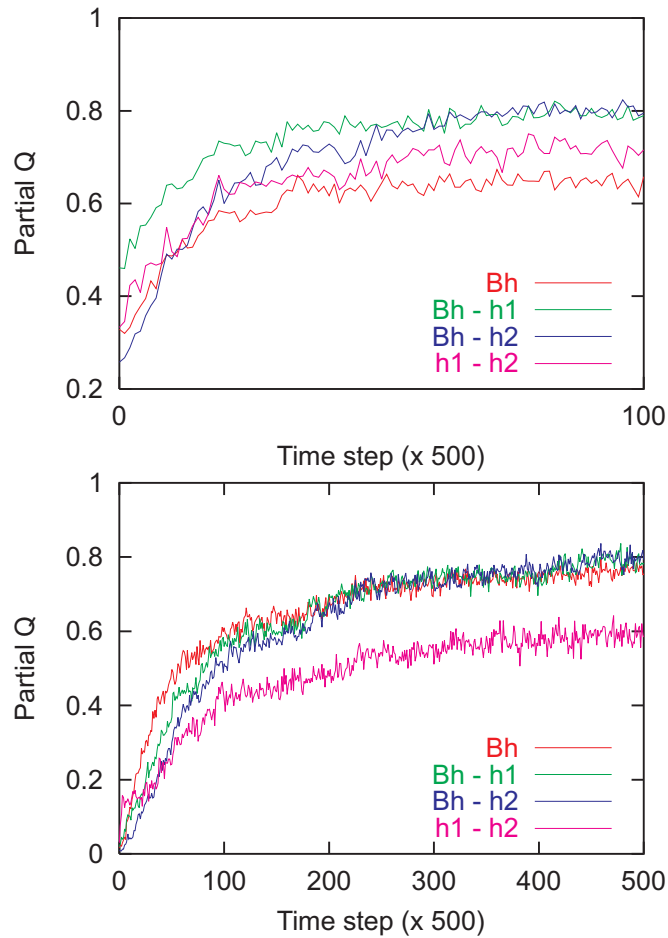


FIG. 5.